OTEC
Vol.25 (2020), 47 ~ 59

The Flow Characteristics Investigation of the S-Shaped Region for Pump-Turbine in Small Guide Vane Opening

Haiyun QIU*[1], Pengcheng GUO*[1], Yoichi KINOUE*[2], Longgang SUN*[1]

*[1] State Key Laboratory of Eco-hydraulics in Northwest Arid Region of China,
Xi'an University of Technology, Xi'an 7, 10048, China
*[2] Institute of Ocean Energy, Saga University, 840-8502, Japan

Abstract

Pumped-storage power station is the most effective regulator in the current power grid. Its core components, pump turbine, requires higher stability and flexibility. But the two unstable regions, which are the S-Shaped characteristic region of the turbine mode and the hump area of the pump mode, become a bottleneck restricting the development of pump turbine and its system. The two unstable regions are also one of the key issues affecting the safety of units and power system. This paper takes a pump-turbine model of a pumped-storage power station as the research object, and conducts a numerical simulation study on the flow characteristics in the S-Shaped characteristic region of the small guide vane opening. By analyzing the flow streamlines and velocity distributions of different span-wises in the runner, it is found that when the pump turbine is operating at partial operating conditions, a vortex structure is formed on the hub side of the runner, a water ring is formed on the middle span-wise, and the back flow forms on shroud side. When the unstable flow structure appears in the runner, the high axial and circumferential velocity appears at the inlet of the runner and larger range of low speed areas appear in the runner passages. The inflow of the runner is obstructed. When the water ring appears on the middle span-wise, the flow around the head of the runner is serious.

Keywords: Pumped-storage power station Pump-turbine S-Shaped characteristics Back flow vortex structures Low frequency pressure pulsation

1. Introduction

Reversible pump-turbine units of pumped storage power stations have the advantages of rapid start-up and frequent conversion of operating conditions, can quickly respond to the needs of the power grid, and play an important role in improving the stability of the power grid (ZUO Z G, 2016). However, as renewable energy sources such as solar and wind energy have entered the power grid in recent years, the stability of the unit has become increasingly prominent (LI D Y, 2018). One of the reasons is that when the pump-turbine is operating in the turbine mode, the S-Shaped characteristic region (SSCR) appears(ZENG W, 2016), which means that when the pump-turbine crosses the runaway point and enters the braking zone, the slope of the characteristic curve is positive and multi-value feature is formed. This multi-value feature can easily induce unstable problems such as start-up difficulty, large pressure fluctuation of load rejection, and even self-excited oscillation during runaway process(XIA L S, 2017). Studies have shown that these instability problems are related to unstable flow structures in the runner and guide vanes, such as backflow, unstable vortex structures, and rotational stall. Therefore, it is necessary to study the correlation between the flow structure and operating stability in the SSCR.

In order to study the instability of pump turbine in SSCR, various reseachers have studied this problem by different methods. Hasmatuchi(HASMATUCHI V,2009), and Guggenberger(GUGGENBERGER M, 2014) et al. conducted the experimental studies on the flow field and pressure pulsation of a low-specific speed pump turbine respectively, and observed the difference in velocity distribution and pressure pulsation in the vaneless zone as well as the dynamic change process of unsteady flow in the SSCR. With the development of computational fluid dynamics, CFD numerical

Date of Manuscript Acceptance 2020.11.20
E-mail of corresponding author: guoyicheng@xaut.edu.cn

simulation has become one of the main methods to study the internal flow characteristics of hydraulic machinery. Sun Longgang (Sun L G, 2019) conducted a numerical simulation study on the internal flow characteristics of the draft tube under the partial load of a Francis model turbine, and analyzed the periodic evolution process of the vortex belt and its induced pressure pulsation characteristics. Gou Dongming (GOU D M, 2018) et al. established a geometric model of the full overcurrent system of a pumped storage power station, and adopted the three-dimensional coupled turbulence calculation method of the combined VOF two-phase flow model and single-phase flow model to conduct a numerical study on the transition process of the runaway in the pump condition, and found that the low-frequency pressure pulsation of the unit in the runaway condition was caused by a large number of vortices in the runner passages. Widmer (WIDMER C, 2011), Cavazzini(CAVAZZINI G,2015), and Wang Leqin (WANG L Q,2011) carried out numerical simulation research on the internal flow field in the SSCR of a pump turbine, and concluded that the guide vane opening (GVO) affects the formation of the vortex in the vaneless region, the unstable vortex in the vaneless region, and the backflow and rotation stall in the runner are related to the S-Shaped of the characteristic curve.

In conclusion, the flow characteristics in the SSCR are one of the current research keys of pump turbine. In order to avoid the appearance of S-Shaped region in engineering, a series of measures have been adopted, among which the early successful method is the misaligned guide vanes (Xiao Y X, 2014). The use of the misaligned guide vanes has a certain improvement on the stability of the pump turbine operating in the SSCR, but at the same time it also generates a strong pressure pulsation inside the unit, which brings new problems to the stable operation of the pump turbine. In order to improve stability or eliminate the influence of the SSCR, it is necessary to study its formation mechanism. The S-Shaped region of the pump turbine is highly correlated with the opening of the guide vane. In this paper, a model of the pump turbine is taken as the research object, and the numerical simulation of the flow characteristics of the S-Shaped region is carried out for the small guide vane opening.

2. Computational methodology

2.1 Pump turbine model

The numerical domain includes spiral case, stay vane, guide vane, runner and draft tube. The runner has a specific speed(n_s) is 21.82 . The ns is defined as follows:

$$n_s = \frac{n\sqrt{Q_{opt}}}{H_{opt}^{3/4}} \tag{1}$$

The inlet of the spiral case and the outlet of the draft tube were extended by $10D_{2m}$ respectively to make the inflow more in line with the actual flow and reduce the vortex intensity at the outlet of the draft tube. Under the optimal operating conditions, the opening degree of the guide vanes is 11°, the unit discharge and the unit speed are Q_{11}=0.4067m /s and N_{11}=34.22r /min respectively, corresponding to the prototype head H_p=675m and the output P_p=357.5MW. The main parameters of the pump turbine model are shown in Table 1, and the geometry of the numerical calculation domain is shown in Figure 1.

Table1 Parameters of model pump-turbine

n_s	Z_r	Z_g	Z_s	D_{1m} (m)	D_{2m} (m)	B_0 (m)	D_0 (m)	n (r/min)
21.82	9	20	20	0.553	0.25198	0.03776	0.66239	1052

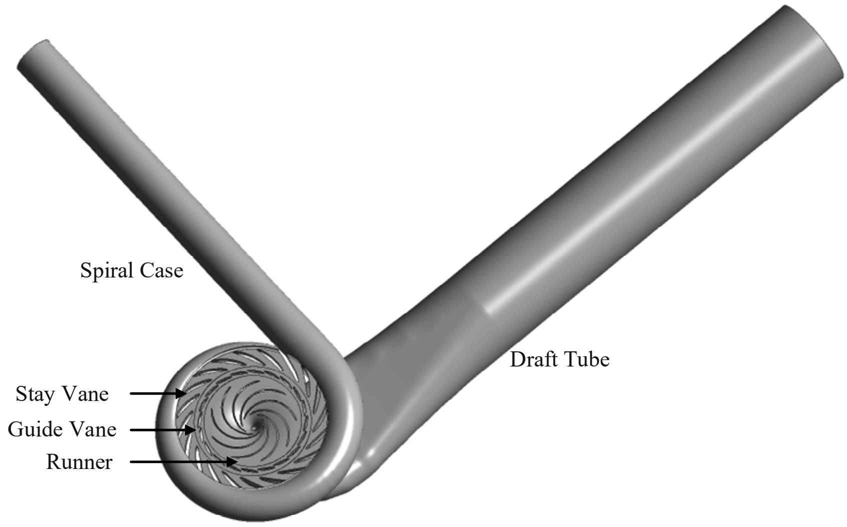

Fig.1 Computational domain

2.2 Mesh

The structured hexahedral mesh is used, which is completed by ICEM-CFD software, and different parts are connected by interfaces. Because the guide vane and the runner is stator and rotor respectively , and the upstream and downstream flows affect each other, the flow is relatively complex in these two domains and the hydraulic loss is relatively large. So in present, the guide vane and runner domain are the key parts for studying with more numbers of mesh than others three parts. Meanwhile, in order to obtain the accurate flow situation near the wall surface, Special refinements were applied at the wall surface of each overflow component, and the schematic diagram of the grid for each component is shown in Fig2.

（a）Spiral Case

（b）Stay Vanes and Guide Vanes

（c）Runner

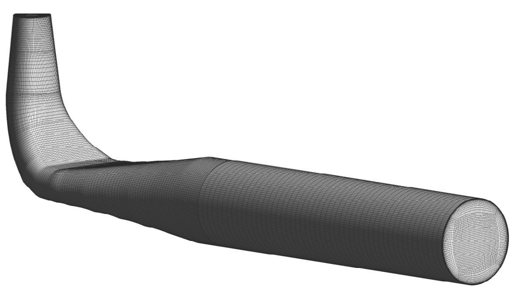

（d）Draft Tube

Fig.2 Schematic diagram of mesh

In order to exclude the influence of the number of grids on the accuracy and credibility of the simulation calculation, The grid independence checks were performed by different sizes of grid with element number from 4.18×10^6 to 10.89×10^6 at the optimal operating points. As shown in Figure 3, when the number of grids is more than 7.18×10^6, the change of the head is not obvious. Considering the numerical accuracy and time cost, the selected total element numbers is 9.5×10^6. The gird parameters used for the simulations are shown in Table 2.

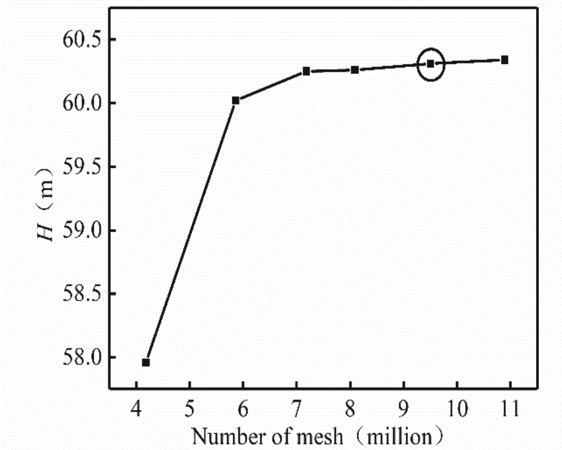

Fig.3 Grid dependence analysis

Table.2 Number and parameters of grid elements

parameters	Spiral case	Stay vanes	Guide vanes	Runners	Draft tube
Number	899954	1484147	3082560	2917701	1119230
Minimum angle（°）	27.4	29	27	26	30
Minimum grid quality	0.37	0.42	0.47	0.43	0.51

2.3 Turbulence Model and Boundary Conditions

The SST *k-ω* turbulence model is used for simulation, which combines the advantages of the *k-ε* model and the *k-ω* model, and can accurately predict the flow near the wall for it applies the *k-ω* turbulence model in the boundary layer domain and the *k-ε* turbulence model in the remaining regions. With the transport equation as follows.

$$\begin{aligned}&\frac{\partial k}{\partial t}+U_j\frac{\partial k}{\partial x_j}=P_k-\beta^{*}k\omega+\frac{\partial}{\partial x_j}[(\nu+\sigma_k\nu_t)\frac{\partial k}{\partial x_j}]\\&\frac{\partial\omega}{\partial t}+U_j\frac{\partial\omega}{\partial x_j}=\alpha S^2-\beta\omega^2+\frac{\partial}{\partial x_j}[(\nu+\sigma_\omega\nu_t)\frac{\partial\omega}{\partial x_j}]+2(1-F)\sigma_{\omega2}\frac{1}{\omega}\frac{\partial k}{\partial x_i}\frac{\partial k}{\partial x_i}\end{aligned}\qquad(2)$$

Where the turbulent viscosity $\nu_t=\dfrac{\alpha_1 k}{\max(\alpha_1\omega, SF_2)}$,F，Pk，β，β^*，σ_k，σ_ω, $\sigma_{\omega2}$,etc. are the closure coefficients of the equations.

The high resolution is used for advection scheme and the Second Order Backward Euler is set for transient scheme. Time step for the simulations corresponds to two degrees of the runner rotation. The maximum number of iterations per time-step was set to 10, and the convergence criteria of the residuals at each time-step were set to 1.0×10^{-3}. The simulation time of every operating point took about 15revolutions and the results of the last 5 revolutions are analyzed.

The boundary conditions were defined as follows: for the turbine operating conditions to the braking conditions, mass flow boundary was prescribed at the spiral case inlet, and static pressure was defined at the draft-tube outlet, and for the reverse pump operating conditions, the boundary conditions for inlet and outlet were charged. The remaining solid walls were specified as the no-slip walls.

3. Results

3.1 Comparisons between the experimental and numerical characteristic curves

When the guide vane opening is 7°, the full characteristic curve of the pump turbine is simulated at a number of points in the first and fourth quadrants, and the result of experiment and simulation are compared, as shown in Figure 4. It obvious that the steady calculation results and the experimental results have S-Shaped region. The numerical simulation results are in good agreement with the experimental results, which demonstrates that CFD simulation settings in the present are reasonable and reliable.

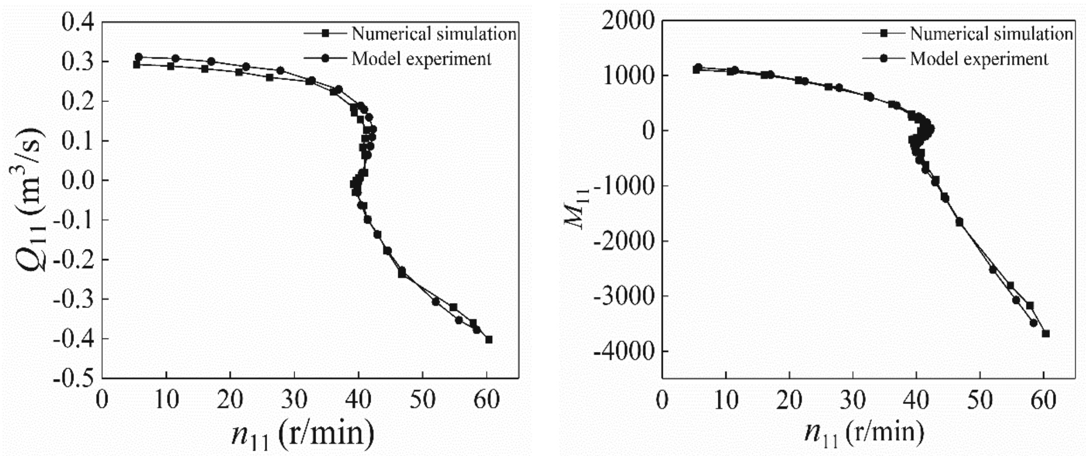

Fig.4 Comparisons between the experimental and numerical characteristic curves
(a) n_{11}-Q_{11} (b) n_{11}-M_{11}

Based on the result of the steady simulation, five operating points were chosen to carry out the unsteady simulations, which locations are shown at the Fig 5.The first operating point($OP1$) is the turbine operating condition, which has large discharge and high efficiency. The second operating point($OP2$) is the turbine operating condition ,too, but is closed to the runaway condition($OP3$). The fourth operating point ($OP4$) is located in the turbine brake region, while the fifth operating point($OP5$) is the reverse operating condition. Guide vane opening is the same for all the considered operating points. The detailed parameters for these operating points are shown in the Table 3.

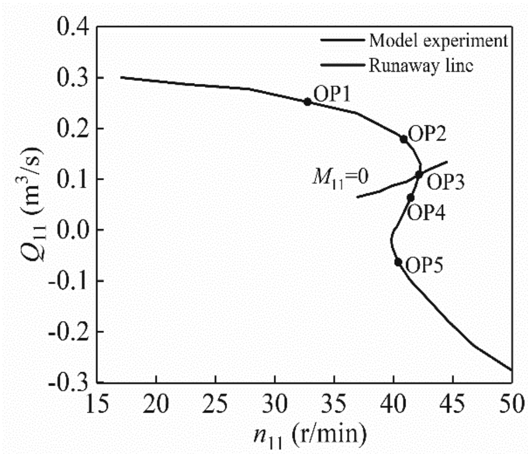

Fig.5 Distributions of the operating points for the unsteady simulations

Table 3 Parameters of the five operating points

Parameters / Operating Points	Operating Conditions	H（m）	n_{11}（r/min）	Q_{11} （m³/s）
OP1	Turbine	21.177	32.76	0.25213
OP2	Turbine	18.501	40.89	0.17858
OP3	Runaway	17.405	42.17	0.10912
OP4	Turbine Braking	17.995	41.47	0.06346
OP5	Reverse Pump	18.944	40.89	-0.06306

3.2 Analysis on the internal flow of runner channels

Runner is the energy conversion part of the pump-turbine, and the internal flow state is closely related to the external characteristics of the pump turbine. In Fig 6, the distributions of the non-dimensional radial velocity component U_r and circumferential velocity component U_t for the different conditions are presented, respectively. The velocity is made non-dimensional by using the runner rotational velocity U=n×π×D$_m$/60. Positive U_r means inflow and negative one means outflow. Positive U_t means that the circumferential velocity is in line with the rotation direction of the runner, and negative Ut means the opposite.

In Fig 6, from the hub to the shroud, U_r is almost positive for OP1 with the features of small in the middle and large at both ends. Except for the reverse pump operating condition(*OP*5), the U_r of the upper runner channel near the hub side increases as well as the high velocity area increases with the change of operating conditions. While for the lower part of runner channel near the shroud side, negative U_r appears which means there is back flow in shroud side. The negative U_r area increases with conditions change, suggests that increasing back flow region. The variation for U_r of OP5 is much smaller than that of other operating conditions, and the velocity coefficient is relatively small. The positive radial velocity area is near the shroud side, but it is almost negative on the hub side and the middle flow surface due to the flow direction is opposite to that of the turbine.

The distribution of the circumferential velocity coefficient is quite different from the radial velocity coefficient. The circumferential velocity coefficients of all operating conditions are positive. For *OP*2 to *OP*4, when a higher radial velocity appears at the hub side, the circumferential velocity also appears a higher value. However, there is little difference in the circumferential velocity distribution at the shroud side. When it operates at *OP*5, the circumferential velocity is smaller than the other four operating conditions, and the distribution is more uniform.

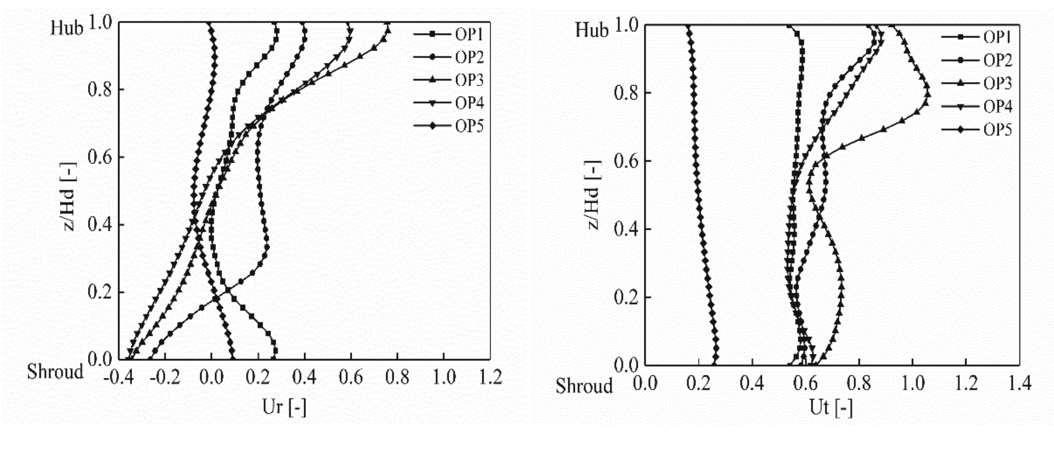

Fig 6 Radial velocity and circumferential velocity distribution at runner inlet

The velocity coefficient distribution at the runner inlet shows that the flow structure is different at different positions in the runner. In order to further understand the change of the flow structure in the runner, the velocity vector, meridional velocity and circumferential velocity of the three span-wise locations in the runner were analyzed under various operating conditions. The meridional velocity and the circumferential velocity are respectively expressed by corresponding velocity coefficient, where the meridional velocity coefficient Um is the ratio of the meridional velocity Vm to the runner rotational velocity.

The velocity vectors together with the flow streamlines and the mean distributions of the non-dimensional meridional velocity U_m and circumferential velocity U_t at 0.1, 0.5, 0.9 span-wise for the five operating points of different span-wise locations are presented in Figures 7, 8, and 9, respectively. As shown in Fig 7, on the 0.1span-wise location, the velocity vectors together with the flow streamlines and velocity distribution of OP1 are uniform, and the flow in the runner is smooth. When operating at OP2, vortex structures appear on the pressure side of leading edge of runner blades, and there are full vortex structures formed in several channels ,while in OP3 and OP4, full vortex structures formed in all runner channels. When operating in OP5, there has no vortex structure in runner inlet, but the inflow of the guide vane outlet and the outflow of the runner inlet converge at the leading edge of the runner blade, bypass the head of blades and flow into the next channel. As a result, an obvious water ring is formed, and the flow separation is severe as well as the small vortices filled in the channels.

The meridional velocity distribution shows that when the vortex structure appears in the runner, a ring-shaped high meridional velocity region is formed before the runner inlet, which is gradually expanded to the entire flow channel with the change of the operating points, indicating that the flow capacity of the runner was decreasing. The inlet of the runner exhibits a higher circumferential velocity, and the negative circumferential velocity region gradually appears on pressure side of blades, which is consistent with the position of the vortex, indicating that the direction of rotation for the vortex is opposite to the direction of rotation for the runner. The high meridional velocity region of the runner inlet almost disappears when it operates at the OP5, the low meridional velocity region expands and almost fill the entire runner channel. And the high meridional velocity region is scattered distribution within the runner channel, wheel that low-velocity region at the exit zone into a high-velocity region. This is because when the pump-turbine is operating at OP5, the inlet and outlet of the runner are opposite to that of turbine operating points. The negative circumferential velocity region in the runner is also increased compared to the other four operating points, mainly distributed in two places, one is the band-shaped area which begins from the head of the suction side of the blade and extend into the runner; another is at the trailing edge of the blade and close to the suction side.

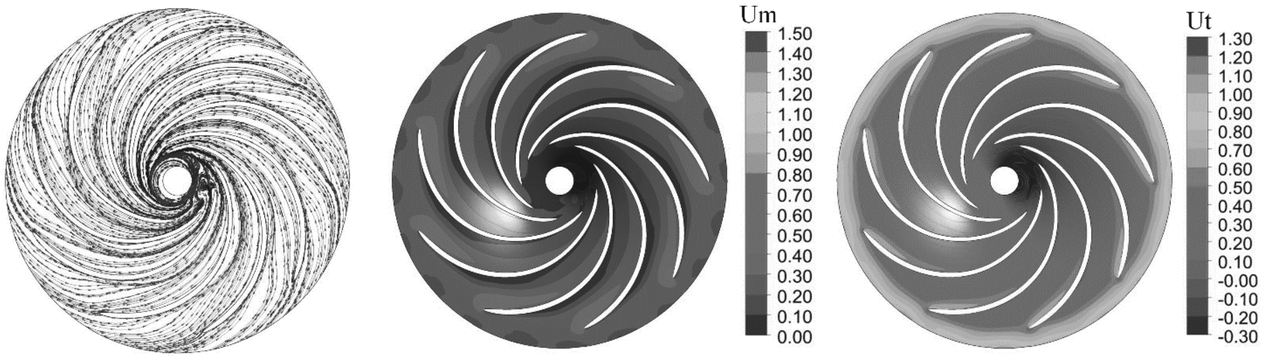

（a）OP1

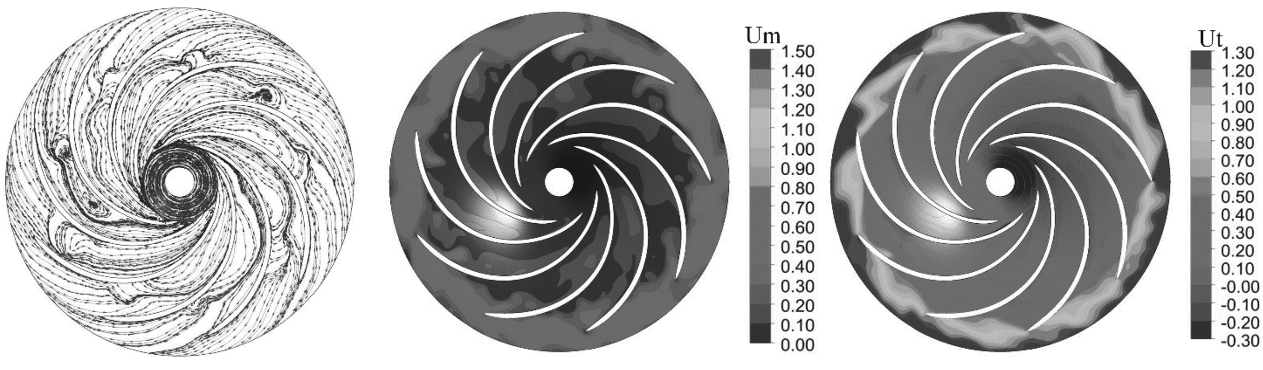

（b）OP2

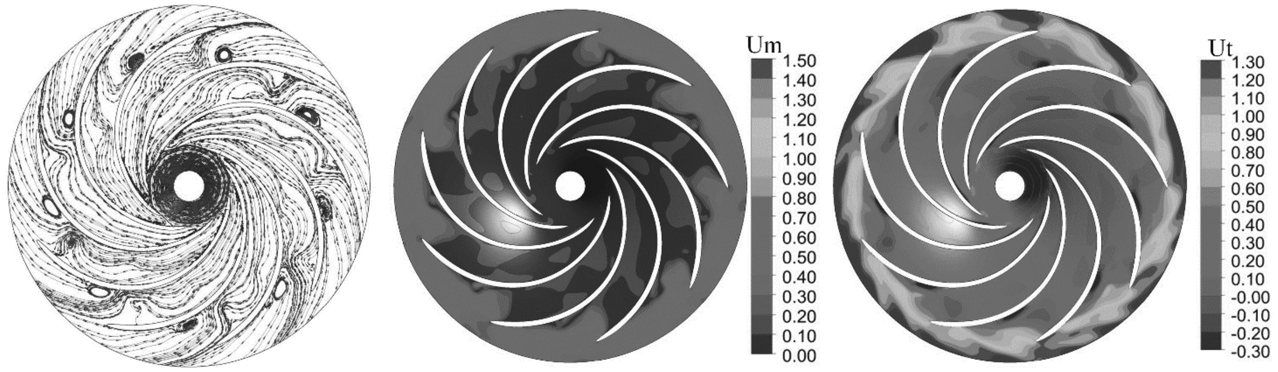

（c）OP3

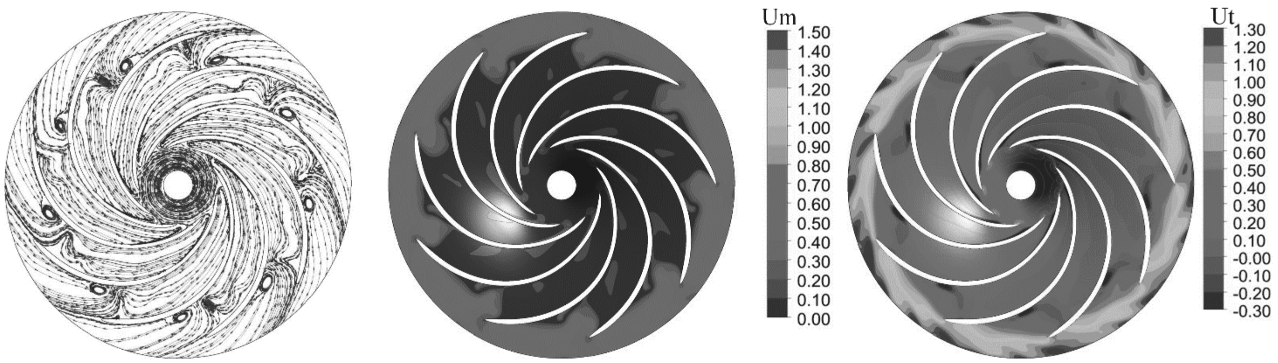

（d）OP4

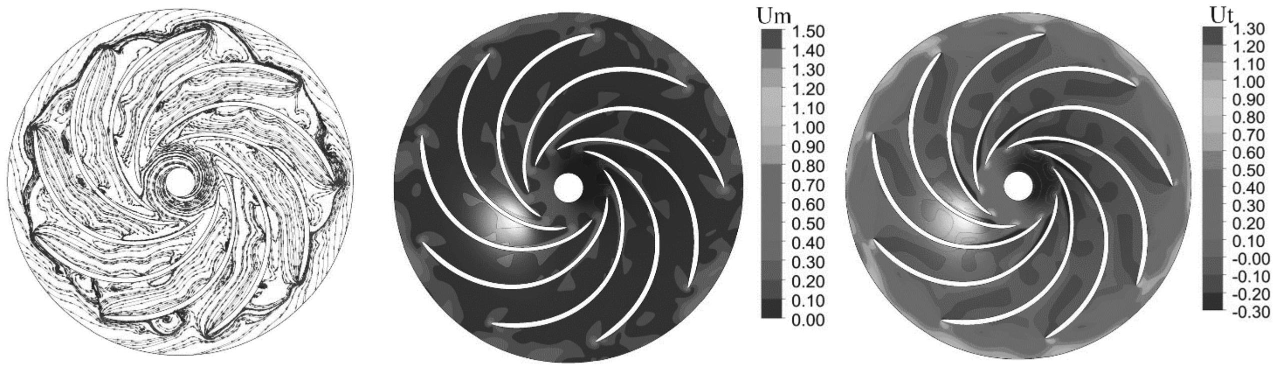

（e）OP5

Fig.7 The velocity vectors together with the flow streamlines and the mean distributions of the non-dimensional meridional velocity Um and circumferential velocity *U*t at 0.1 span-wise of the five operating points

On the 0.5 span-wise locations, the velocity vectors together with the flow streamlines and velocity distribution of OP1 do not change much, and the velocity distribution shows that the meridional velocity is greatly affected by rotor-stator interference. When operating at off-design condition, the structure is changed, as shown in figure 8, a ring-shaped flow appears in the vaneless area before the runner inlet from OP2. The ring-shaped flow is divided into two parts when flowing through the runner inlet, one part of the fluid flows downstream along the runner channel, and the other part flows counterclockwise in the circumferential direction to the next runner blade head and bypasses the head to enter the next runner channel, so a cross flow is formed at the runner inlet t. The existence of the flow around makes the local high meridional velocity and circumferential velocity area exist at the head of runner. Incomplete vortex structures appear in part of the runner channels, and the scattered low meridional velocity region is distributed in the runner, which indicates that the flow in the runner is disturbed. With the change of operating conditions, the density of the ring-shaped flow in the bladeless area before the runner is enhanced to form a complete water ring. The cross flow at the inlet of the runner and the vortex structure on the pressure side become obvious. In terms of velocity distribution, the low meridional velocity area within the runner and in the front of the runner area is increased. When operating at OP4, the runner channel is almost completely covered by the low meridional velocity, indicating that the runner flow is greatly hindered. On the pressure side of the runner blade, there is a negative circumferential velocity corresponding to the vortex position.

Affected by the cross flow, nine distinct high circumferential velocity zones are formed at the head of the runner. While entering the reverse pump condition, the water ring in the bladeless area before the runner disappears, but there is still turbulence and a significant meridional velocity zone at the head of the runner. There are a large number of small vortices at the runner outlet, which cause the high meridional velocity region at the runner outlet. The circumferential velocity distribution on middle span is similar to that on the hub side that a negative meridional velocity band is formed from the pressure side of the runner head into the runner ,and the high meridional velocity region is formed at the outlet of runner.

Compared with the flow on the hub side, when running under off-design conditions, the ring-shaped flow appearing on the middle spin-wise of the runner gradually forms the water ring and the cross flow, and the vortex structure gradually appears on the pressure side of the runner inlet. Because the water ring and cross flow exist in the inlet of runner, the head turbulence of the runner is aggravated, and the local high circumferential velocity area is formed at the runner inlet. While when the vortex structure is gradually formatting, the flow capacity of the runner of is decreasing. The low meridional velocity area at the inlet and outlet of the runner and the area inside the runner are increased, indicating that the flow is blocked. The blocking water ring on the middle spin-wise of the runner disappeared at OP5, but the turbulence at the head of the runner was still relatively strong.

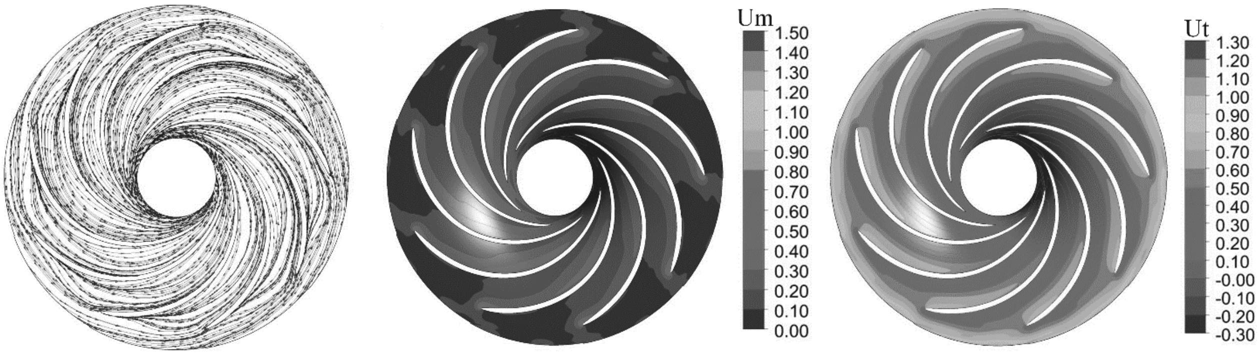

（a）OP1

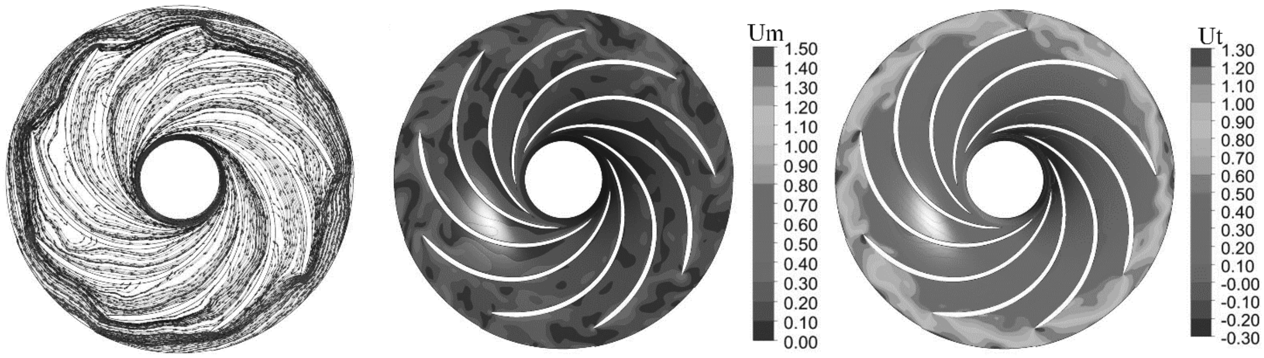

（b）OP2

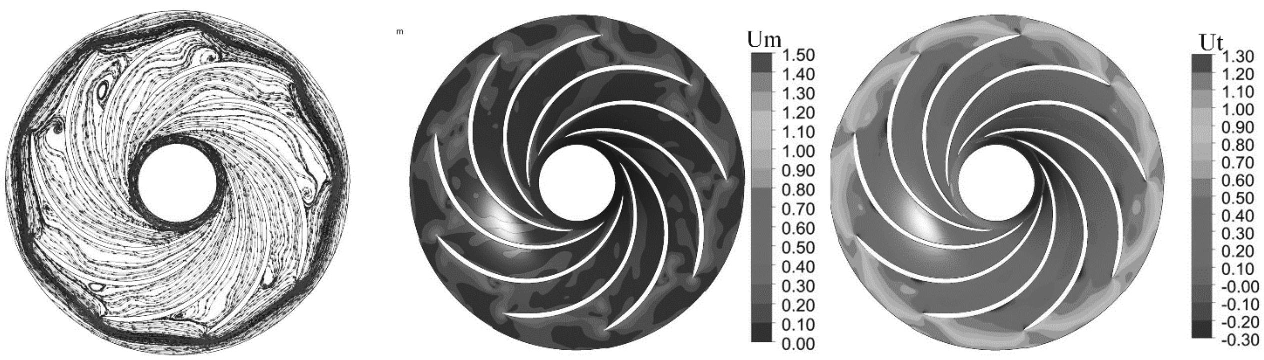

（c）OP3

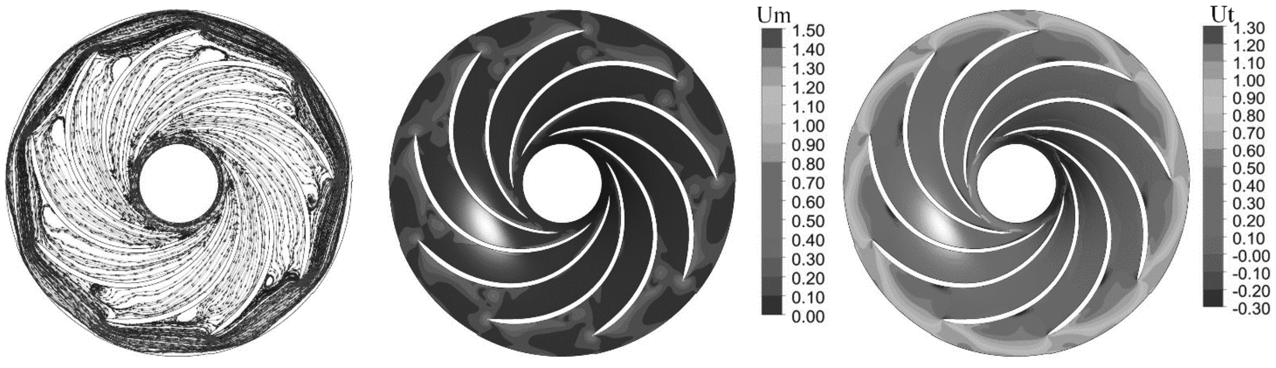

（d）OP4

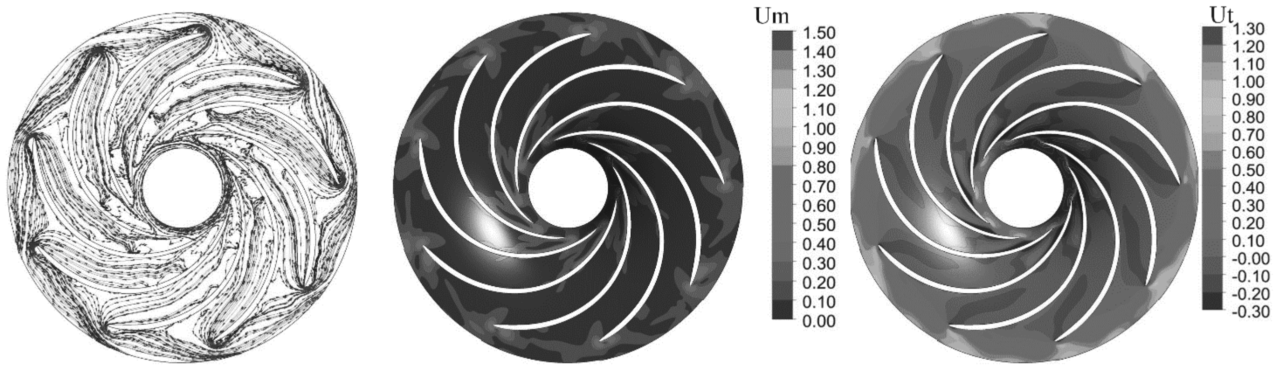

（e）OP5

Fig.8 The velocity vectors together with the flow streamlines and the mean distributions of the non-dimensional meridional velocity U_m and circumferential velocity U_t at 0.5 span-wise of the five operating points

As shown in Fig 9, on the 0.9 span-wise location, the flow state of the OP1 on the hub side is basically the same as that on the shroud, indicating that the flow in the runner is basically uniform and symmetrical at OP1. Compared with the flow on the 0.5 span-wise location, no water ring is formed in the vaneless area before the blade at the shroud side, but there is still a circulation with the greatly weakened strength. Besides the circulation is deflected upstream to form a backflow in the vaneless area. The distribution of the radial velocity coefficient of the runner inlet in the direction of the blade height above shows that under OP2 to OP4 conditions, the radial velocity coefficient at the shroud side is negative, which shows that the backflow occurs at the shroud side. It can be seen that the local high circumferential speed of the vaneless area before the runner is caused by backflow. The vortex structure formed on the hub side of the runner is no longer obvious on the shroud side, but there is still flow separation on the pressure side of the runner blade. Different from the other four operating conditions, the reverse pump forms complete vortex structures at the outlet of runner. Affected by the vortex structure, from the hub to the shroud side, the low meridional velocity area at the runner exit disappears, gradually forming a larger range of high meridional velocity, while the circumferential velocity distribution does not change much. It shows that the area where the runner blades transfer energy to the fluid as the pump works gradually decreases from the shroud to the hub side.

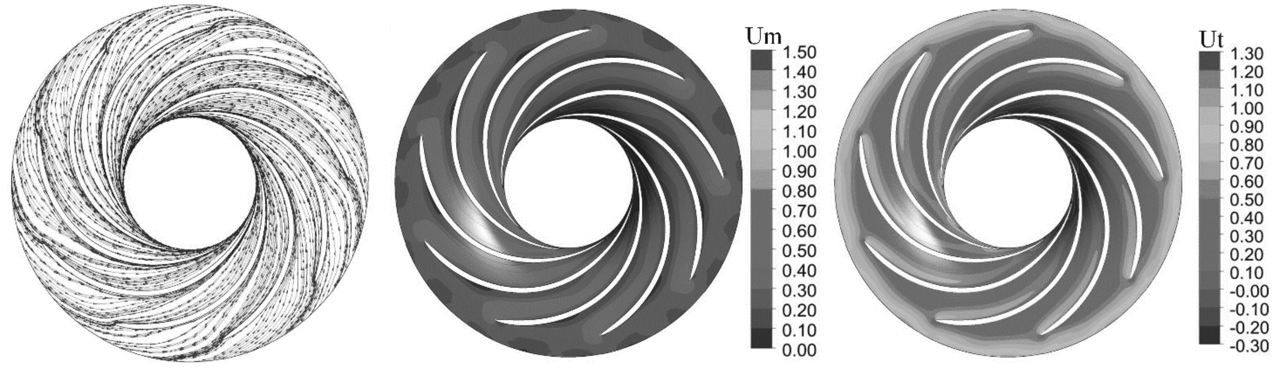

（a）OP1

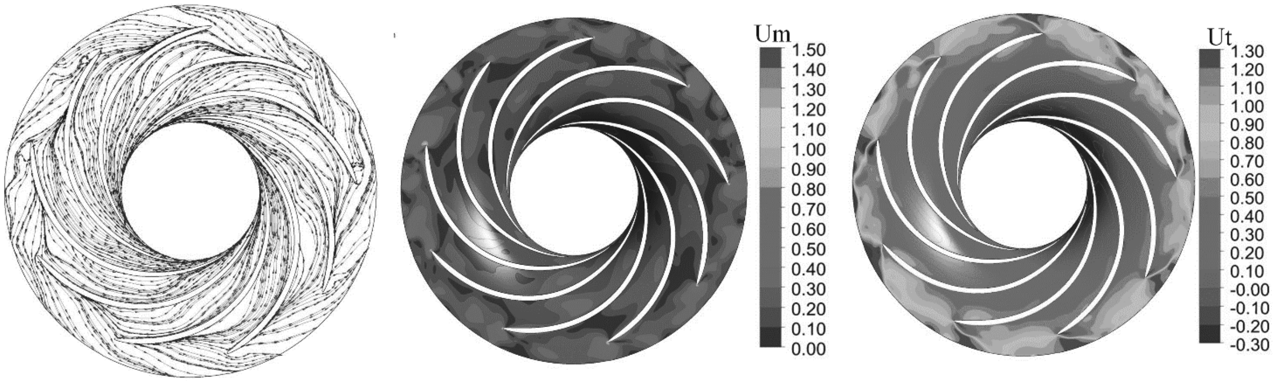

（b）OP2

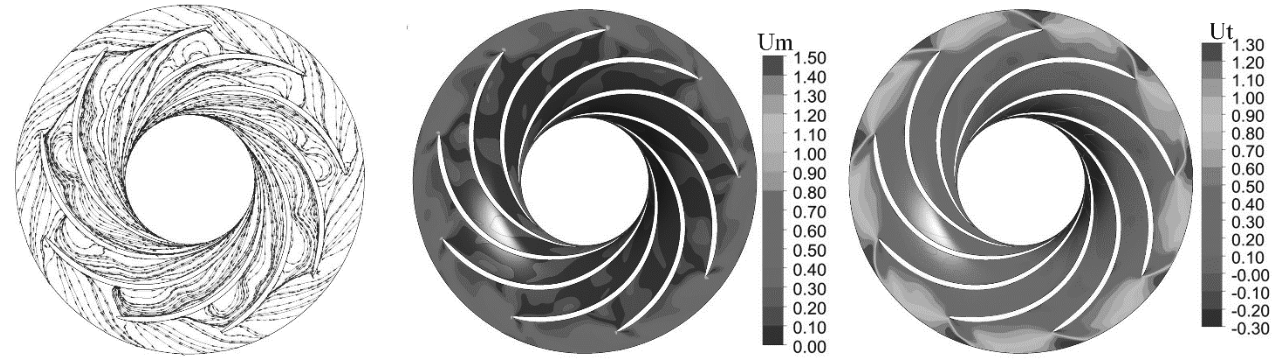

（c）OP3

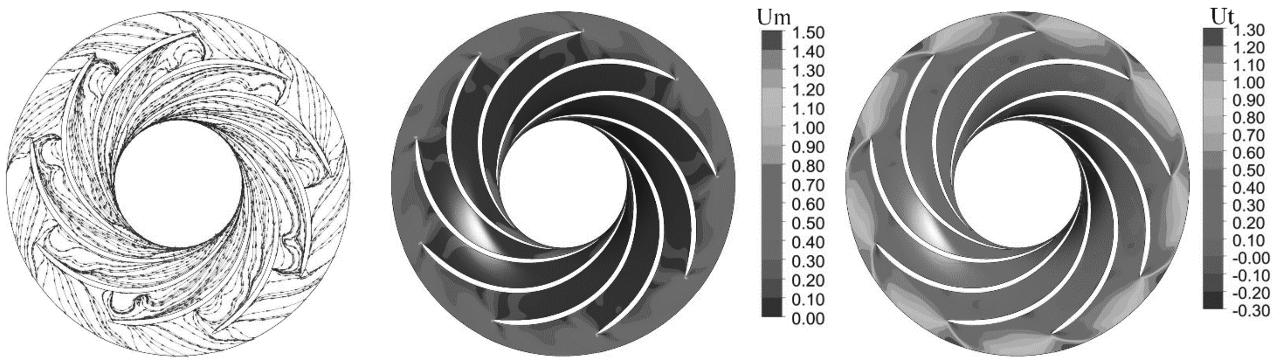

（d）OP4

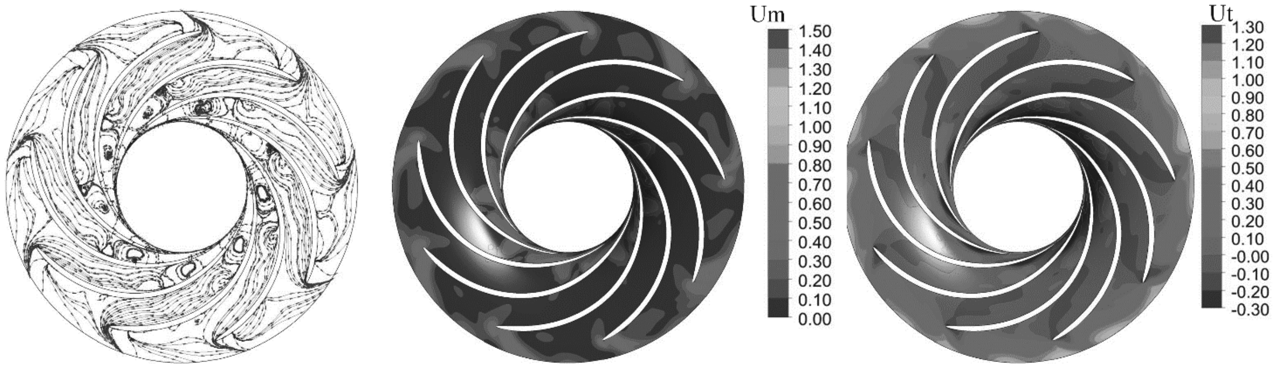

（e）OP5

Fig.9 The velocity vectors together with the flow streamlines and the mean distributions of the non-dimensional meridional velocity Um and circumferential velocity Ut at 0.9 span-wise of the five operating points

The above analysis shows that the vortex structure forms at the hub side of the runner and basically disappears at the shroud side of the runner with the change of operating points from turbine mode to the braking mode. In order to further illustrate the change in the flow structure of the runner inlet along the direction of the blade height, a three-dimensional streamline diagram of a runner channel under OP3 operating conditions is analyzed, as shown in Fig 10. The inflow on the hub side bends downward at the inlet of the runner near the pressure surface and is divided into two parts of fluid. One part forms a vortex structure inside the runner. After the vortex structure is developed inside the runner, it almost disappears at the shroud side and eventually flows downstream with the mainstream. Another part of flow has a tendency to flow upstream during the flow to the shroud side, so that a part of the fluid bypasses the runner head and enters the vaneless area at the middle flow surface, forming a high-speed water retaining ring and a cross-flow structure, which hinders the inflow, reduces the inflow, and has a great influence on the speed distribution of the runner inlet. And there is also a part of the fluid flows to the shroud side and forms the backflow structure. On the external characteristic curve, OP2 and OP5 are in the operating region with negative slope, while OP3 and OP4 are in the region with positive slope. When there is an unstable flow structure in the runner, the inflow of the runner is blocked. As the speed increases, the flow rate decreases, the vortex structure, the water retaining ring structure, and the backflow structure of the runner inlet form a complete unstable structure, which further blocks the flow, causing the pump turbine to be unable to maintain operation at low discharge with higher speeds. Therefore, the rotation speed is reduced, and the S-Shaped region appears after the runaway point on the characteristic curve.

Fig.10 Three-dimensional schematic diagram of flow structure changes at the inlet of the runner

4. Conclusions

By analyzing the flow structure in the runner, it is found that, except for OP5 condition, vortexes occur at the hub side of the runner with the change of operating condition, a water retaining ring appears at the middle flow surface, and a backflow occurs at the shroud side. When the unstable structure appears in the runner, the high velocity area is formed at the head of the runner blade, and a large range of low velocity area appears in the runner passages. When operating at OP5, the water retaining ring appears at the hub side, the vortex structure appears at the runner outlet, which is strongest near the shroud side. Besides the flow separation in the runner is serious, and both the meridional velocity and circumferential velocity are less than that at other operating points, but the range of the low velocity area is the largest. The existence of unstable flow structure in the runner reduces the flow capacity of the runner, making the pump turbine unable to maintain operation at low discharge with higher speeds. As a result, the runner's speed decreases, and the characteristic curve shows an S-Shaped region before and after the runaway condition.

Acknowledgment

This work was supported by the National Natural Science Foundation of China (Grant No. (51839010), the Key Research and Development Program of Shaanxi Province (Grant No. 2017ZDXM-GY-081), the Youth Innovation Team of Shaanxi Universities (Grant No. 2020-29), and the cooperative Research Program of IOES (No.18A07).

References

ZUO Z G, FAN H G, LIU S H, et al. S-shaped characteristics on the performance curves of pump-turbines in turbine mode – A review. Renewable and Sustainable Energy Reviews, Vol.60, (2016), pp.836-851.

LI D Y, WANG H J, QIN Y L, et al., Numerical simulation of hysteresis characteristic in the hump region of a pump-turbine model. Renewable Energy, Vol.115, (2018), pp.433-447.

ZENG W, YANG J, YANG W. Instability Analysis of Pumped Storage Stations Under No-Load Conditions Using a Parameter-Varying Model. Renewable Energy, Vol.90, (2016), pp.420–429.

XIA L S, CHENG Y G, YANG Z Y. Evolutions of pressure fluctuations and runner loads during runaway processes of a pump-turbine. Journal of Fluids Engineering, Vol.139, No.9, (2017).

HASMATUCHI V. Experimental investigation of a pump-turbine at off-design operating conditions. Brno: International Meeting of the workgroup on Cavitation and Dynamic problems in Hydraulic Machinery and Systems, (2009).

GUGGENBERGER M, SENN F, SCHIFFER J. Experimental investigation of the turbine instability of a pump-turbine during synchronization. IOP Conference Series: Earth and Environmental Science, Vol.22, No.3, 2014.

Sun L G, Guo P C, LUO X F. Investigation on synchronous and asynchronous characteristics of pressure fluctuations towards processing vortex rope in Francis Turbine draft tube. Chinese Journal of Agricultural Machinery, Vol.50, No.9, (2019), pp.122-129.

GOU D M, GUO P C, LUO X Q. 3-D combined simulation of power-off runaway transient process of pumped storage power station under pump condition. Hydrodynamics Research and Progress, Vol.33, No.1, 2018, pp.28-39.

WIDMER C, STAUBLI T. LEDERGERBER N. Unstable Characteristics and Rotating Stall in Turbine Brake Operation of Pump-Turbines. Vol.133, No.4, (2011).

CAVAZZINI G, COVI A, PAVESI G. Analysis of the Unstable Behavior of a Pump-Turbine in Turbine Mode: Fluid-Dynamical and Spectral Characterization of the S-shape Characteristic. Vol.138, No.2, (2015).

WANG L Q, YIN J L, JIAO L. Numerical investigation on the “S” characteristics of a reduced pump turbine model. Science China Technological Sciences, Vol.54, No.5, (2011), pp.1259-1266.

Xiao Y X, Wang Z W, Zhang J, et al. Numerical predictions of pressure pulses in a Francis pump turbine with misaligned guide vanes. Journal of Hydrodynamics, Vol.24, No.2, 2014, pp.250-256.